12^{th} International Conference on Fracture Mechanics of Concrete and Concrete Structures
FraMCoS-12
B.L.A. Pichler, Ch. Hellmich, P. Preinstorfer (Eds)

https://doi.org/10.21012/FC12.1253
MS11:6

PROBABILISTIC SERVICE LIFE PREDICTION OF CHLORIDE INDUCED CORROSION UNDER SUSTAINED MECHANICAL LOADING USING MULTIPHYSICAL MODELING

GEREON S. WILDERMANN*, ANNIKA L. SCHULTHEIß*, RAVI A. PATEL* AND FRANK DEHN*

* Karlsruhe Institute of Technology (KIT), Institute of Building Materials and Concrete Structures (IMB)
Gotthard-Franz-Str. 3, 76131 Karlsruhe, Germany
e-mail: gereon.wildermann@kit.edu, www.betoninstitut.de

Key words: Chloride-induced corrosion, sustained mechanical loading, multiphysical modeling, mesoscale modeling, service life prediction

Abstract. Chloride-induced rebar corrosion significantly affects the durability of reinforced concrete engineering structures. The service life in such environment is defined by the time at which a critical chloride content is reached at the reinforcement. For design and maintenance stage prediction of the service life is very crucial. Mechanical loading can significantly impact chloride transport and consequently service life predictions. Therefore, a accurate service life prediction model accounting for multiphysical coupling between chloride ingress and mechanical loading is needed. This study develops a numerical service life prediction model for chloride ingress under sustained mechanical loading. This is accomplished by coupling an elastic scalar damage based mechanical model with chloride diffusion transport model. The coupling accounts for the influence of the local stress-strain field and the damage on the effective diffusion coefficient. The numerical model resolves coarse aggregates (meso-scale) to capture the heterogeneous nature of concrete. Consistent distribution function of input parameters are used to enable probabilistic service life analysis by Monte Carlo method. The developed model is applied to a hypothetical case study which demonstrates a first service life prediction considering different loading scenarios of concrete structures.

1 INTRODUCTION

Chloride ingress in reinforced concrete structures poses a significant challenge due to its potential to cause depassivation of the reinforcement leading to its corrosion. Chloride ingress from the concrete surface is generally treated as a one-dimensional diffusion process. Due to this assumption, traditional probabilistic chloride models, such as given in *fib* Model Code for Service Life Design [1], are limited to uncracked concrete. Mechanical loading however introduces micro cracks into the concrete, which lead to a multi dimensional diffusion process. Therefore, service life prediction models with multiphysical coupling between mechanical loading and chloride ingress is essential for more accurate service life predictions.

Several experimental studies have showed the influence of the loading state on the chloride ingress. The setups of the experiments consist of the application of a defined long-term deformation and subsequent exposure to chlorides. In cases when the concrete was under tension [2–8], the (apparent) diffusion coefficient increases monotonically with increasing load in all experiments. This effect is even more pronounced for the cases where the threshold stress level for micro-cracking is surpassed. For

specimens under compression [6, 7, 9–12] a decrease of (apparent) diffusion coefficient for low stress states was observed in most cases. When the loading threshold for micro-cracking in concrete is exceeded, the apparent diffusion coefficients are either similar, higher or lower compared to the uncracked state; however, most experiments indicate an overall increase in diffusivity [12]. In addition to the changes in the (apparent) diffusion coefficient, some studies [6, 8, 11] demonstrate the influence of loading on the total chloride surface concentration, while it has been shown that the damage does not affect the chloride binding isotherm [6].

By considering the effects of micro- and macro-cracking on chloride diffusivity at given load-induced stress levels, reinforced concrete structures can be also optimized for durability.

This study investigates the influence of mechanical loading on chloride-induced depassivation of reinforcement in concrete using a mesoscale model. A case study of a laboratory scale beam is used to investigate the impact of different loading scenarios and concrete qualities on service life predictions. This study only considers fully saturated chloride transport conditions relevant for concrete structures submerged in seawater.

2 METHODS

All numerical simulations in this study are conducted using COMSOL Multiphysics 6.2 [13].

2.1 Mechanical modeling based on continuum damage mechanics

To model concrete on a mesoscale, the material is divided into coarse aggregates (4 mm $<$ $\varnothing$ $<$ 16 mm), mortar (containing fine aggregates) and the interfacial transition zone (ITZ). The aggregates are assumed to have a circular shape and are randomly distributed in the concrete. It is assumed that the damage occurs exclusively in the mortar or ITZ but not in the aggregates. This is due to the higher strength of the aggregates compared to the surrounding mortar and the even weaker ITZ. In this study, the normal tensile strength of the ITZ is set to 70 % of the mortar's tensile strength, ensuring that failure initiates in the ITZ. The scalar damage parameter d is calculated using the Mazars damage model [14]. In this model, the weighting functions α_t and α_c account for the stress state, while the parameter β governs the contribution of shear effects. The softening behavior under tensile and compressive loading is described by damage evolution functions provided in Eq. 3 and Eq. 4 [14].

$$\sigma_d = (1-d)\sigma = (1-d)C : \epsilon_{el} \tag{1}$$

$$d = \alpha_t^\beta \cdot d_t + \alpha_c^\beta \cdot d_c \tag{2}$$

$$d_t = 1 - (1-A_t)\frac{\varepsilon_0}{\kappa} - A_t e^{-B_t(\kappa-\varepsilon_0)} \tag{3}$$

$$d_c = 1 - (1-A_c)\frac{\varepsilon_0}{\kappa} - A_c e^{-B_c(\kappa-\varepsilon_0)} \tag{4}$$

For localization of the damage the implicit gradient model by Poh and Sun [15] is used, which shrinks the damage zone to a narrow band in higher damaged areas.

$$\tilde{\varepsilon} = \sqrt{\langle\varepsilon_{el}\rangle : \langle\varepsilon_{el}\rangle} \tag{5}$$

$$\bar{\varepsilon} - \nabla \cdot \left(\ell^2(d)\nabla\bar{\varepsilon}\right) = \tilde{\varepsilon} \tag{6}$$

$$\ell(d) = \ell_0\sqrt{\frac{(1-\rho)e^{-\lambda d} + \rho\, e^{-\lambda}}{1-e^{-\lambda}}} \tag{7}$$

The damage within the ITZ is modelled using the approach described in Seetharam et al. [16]. Here, damage initiation and progression are based on the relative displacement components in both normal and tangential directions, with the mixed-mode displacement, calculated as a combination of these components. This approach enables damage tracking analogous to an equivalent strain. The model applies a linear traction-separation law, in which the initial and full decohesion displacements are derived using maximum stress values and a penalty stiffness factor for each mode. The determined mixed-mode decohesion displacement incorporates a mixed-mode exponent to describe the evolving separation between the phases. The stress-relative displacement relations for normal and tangential components in the ITZ involve secant

stiffness terms that adapt as damage progresses. Thus, the model dynamically accounts for the stiffness reduction over the damage process, facilitating a realistic representation of the ITZ response under complex loading.

In this study, the numerical elastic scalar damage based mechanical analyses are conducted in a 2D plane-strain formulation. A stationary solver with an auxiliary sweep is employed to simulate the stepwise loading of the samples.

2.2 Reactive transport model for chloride diffusion

Chloride diffusion is modeled using a single component reactive transport model as described in a previous study for uncracked concrete [17]. For the proposed model, the following assumptions are made: (1) Chloride transport occurs only through diffusion. (2) The ITZ is neglected in the diffusion model, since it was shown for OPC concretes that its influence is negligible [18]. (3) No electro-kinetic effects occur. (4) Chloride ingress does not lead to any other degradation effects (e. g. leaching) of the concrete. (5) The concrete is fully saturated, uniform, and homogeneous. (6) Some chloride ions can be bound by hydration products. Under these assumptions, the chloride transport can be described by Fick's second law:

$$\frac{\delta\left(\phi \cdot C\right)}{\delta t} + \frac{\delta C_b}{\delta t} = \nabla(D_e \nabla C) \tag{8}$$

where C is the aqueous concentration of chloride [$\mathrm{mol/m^3}$ pore solution], D_e is the effective diffusivity of chlorides [$\mathrm{m^2/s}$], ϕ is the porosity [$\mathrm{m^3}$ pores/$\mathrm{m^3}$ concrete], and C_b is the concentration of chlorides in solid phase [$\mathrm{mol/m^3}$ solid]. The chloride concentration in the concrete is evaluated with Eq. 9 in [w. % cement], which is the unit commonly used by engineers.

$$C_{total} = \frac{C \cdot \phi_{mortar} \cdot M_{Cl} + C_b \cdot m_{paste}}{m_{binder}} \tag{9}$$

where $M_{Cl} = 35.453 \cdot 10^{-3}$ kg/mol is the molar mass of chloride, and the masses per $\mathrm{m^3}$ mortar m_{paste} [$\mathrm{kg\,paste/m^3}$ mortar] and m_{binder} [$\mathrm{kg\,binder/m^3}$ mortar]. The effective diffusion coefficient D_e [$\mathrm{m^2/s}$] of Portland cement (OPC) based concrete can be estimated using an Archie-type relationship as given by Seetharam et al. [19]:

$$D_e = D_0 \cdot \phi_{paste}^6 \cdot V_{cp} \tag{10}$$

where $D_0 = 2.03 \times 10^{-9}$ [$\mathrm{m^2/s}$] is the diffusion coefficient of chloride ions in free bulk water, V_{cp} [-] is the volume fraction of the paste in mortar, and ϕ_{paste} [$\mathrm{m^3}$ pores/$\mathrm{m^3}$ paste] is the total porosity of the paste. The latter is estimated using Powers model [20], with the maximal degree of hydration calculated based on the water-binder ratio (w/b) as described in [21] .

Empirical binding isotherms describe the relationship between free and bound chlorides (C, C_b) at a given temperature. In this study Langmuir isotherms are used to account for the bound chloride C_b [g Cl/g phase] of the AFm phase and calcium-silicate-hydrate (C-S-H):

$$C_{b,phase} = \frac{a \cdot C}{1 + b \cdot C} \tag{11}$$

where for C in [mol/l] the parameters a [-] and b [-] are given in Table 1.

Table 1: Parameter of Langmuir isotherms from [17]

Phase	a	b
AFm	0.08	0.57
C-S-H	0.04	2.43

To predict the amount of bound chlorides $C_{b,\text{paste}}$ [g Cl/g paste], the combined binding isotherm for the cement paste can be obtained by combining isotherms of AFm and C-S-H phase as given in Eq. 12.

$$C_{b,\text{paste}} = C_{b,\text{AFm}} \cdot m_{\text{AFm}} + C_{b,\text{CSH}} \cdot m_{\text{CSH}} \tag{12}$$

Consequently, for mortar matrix the binding isotherm is given as

$$C_b = C_{b,\text{paste}} \cdot V_{cp} \cdot \rho_{\text{paste}} \tag{13}$$

where m_{AFm} and m_{CSH} are the mass fractions of AFm and C-S-H phases in the cement paste and ρ_{paste} [kg/m^3] is the density of the cement paste, which can be predicted using thermodynamic modeling (further details see [17]).

In this study, the time-dependent chloride diffusion is numerically simulated on a two-dimensional domain using an implicit solver based on the backward Euler scheme.

2.3 Coupling of mechanical and reactive transport model

As explained in Section 1, the mechanical loading impacts the diffusion coefficient. This influence depends on whether the element is under compression or under tension and whether the internal stress state has exceeded the critical threshold levels which would result in micro cracking. To account for these experimental observations, two modifications are proposed for the transport model based on the stress state computed by the mechanical model. The first modification accounts for the influence of cracking (micro- and macro-cracking) on porosity and in turn on the diffusion coefficient. A linear increase of the porosity, given in Eq. 14, due to damage is assumed as a simplifying approximation.

$$\phi_{paste,d} = \phi_{paste} + (1 - \phi_{paste}) \cdot d \qquad (14)$$

The second load dependent modification accounts for the change of the diffusion coefficient, that is not induced by micro-cracking.

Many studies [5, 9, 10, 22, 23] have presented corelation between uniaxial tensile and compression stress levels and normalized diffusion coefficients for different loading magnitude. Figure 1 and Figure 2 illustrate existing correlations for compression and tension, respectively. In compression diffusion coefficient in general reduces with increase in load for upto a critical load level. Beyond this, microcracking occurs and consequently increase in diffusion coefficient in observed. In contrast, increasing loading under tension leads to an increase in the value of diffusion coefficient.

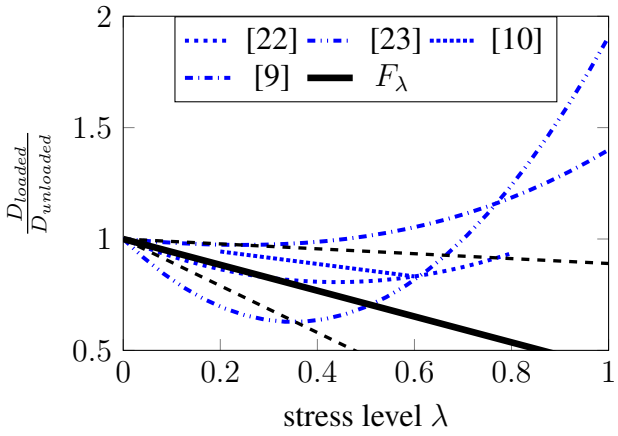

Figure 1: Fitting of F_λ with functions for uniaxial compression

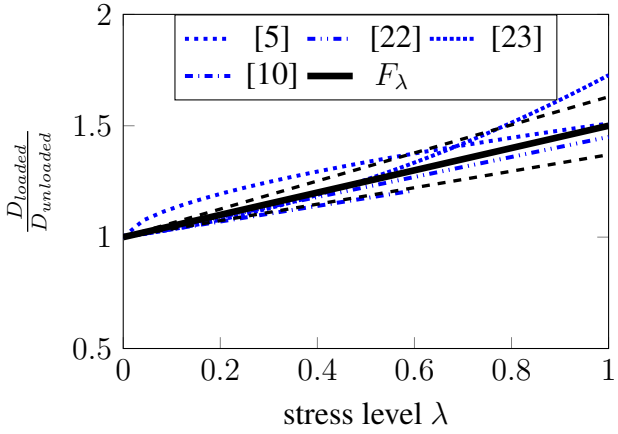

Figure 2: Fitting of F_λ with functions for uniaxial tension

To describe the influence of loading before damage initiation occurs, the stress influence factor F_λ, simplified as given in Eq. 15, accounts for the applied stress level λ.

$$F_\lambda = 1 + sign(I_1) \cdot c_\lambda \cdot \lambda \qquad (15)$$

In the proposed relation, stress influence factor F_λ is described with by a linear function with its slope c_λ. The sign of the second term is determined by the sign of first invariant I_1 of the stress tensor. The value of c_λ is fitted with the uniaxial correlation between normalized diffusion coefficients and stress levels presented in [5, 9, 10, 22, 23]. For fitting, the range

of stress level was limited to maximum 0.4 for compression [24], and to maximum 0.7 for tension [25] in order to neglect the influence of micro-cracking, which in current model is accounted by change in the porosity as given by Eq. 14. For probabilistic analyses, normal distribution was assumed for the value of c_λ as summarized in Table 2.

Table 2: Normal distribution of c_λ

case	mean	std
$I_1 < 0$	0.54	0.43
$I_1 = 0$	0	0
$I_1 > 0$	0.5	0.13

As experimental relationships are derived for uniaxial stress levels, the relationship needs to be transferred on multi-axial states of stress to be applicable for the local stress states in the mesoscale model. Therefore, the stress level λ is defined as the ratio of the first invariant I_1 and the uniaxial compressive strength f_{cm} or tensile strength f_{ctm}, respectively, as given by Eq. 16.

$$\lambda = \begin{cases} \frac{-I_1}{f_{cm}} & , I_1 < 0 \\ 0 & , I_1 = 0 \\ \frac{I_1}{f_{ctm}} & , I_1 > 0 \end{cases} \tag{16}$$

To prevent suprious values of diffusion coefficient, $F_\lambda \geq 0$.

The effective diffusion coefficient under loading conditions is thus predicted by combining the effective diffusion coefficient from Eq. 10 with the stress influence factor F_λ and the increased porosity due to damage $\phi_{\text{paste,d}}$.

$$D_{e,load} = F_\lambda \cdot D_0 \cdot \phi^6_{\text{paste,d}} \cdot V_{cp} \tag{17}$$

In order to perform the coupling, the mechanical problem is solved first. Then one way coupling is assumed to calculate the diffusion coefficient $D_{e,load}$ following Eq. 17 based on the stress field. During the chloride diffusion simulation, the diffusion coefficient is not further changed.

2.4 Probabilistic modeling

Probabilistic analysis is crucial for assessing the impact of stress on chloride ingress in concrete because it accounts for the inherent variability and uncertainty in material properties such as porosity and phase composition, and modeling uncertainties. In this study, the limit state of the service life prediction is the limit state of chloride-induced depassivation p_{dep}, where the critical chloride concentration is exceed at specific depth x [1]:

$$p_{dep} = p(C_{crit} - C(x,t)_{max} < 0) \tag{18}$$

Before the probabilistic evaluation, the damage and stress state is calculated for a defined loading scenario as described in Section 2.1. Then Monte Carlo simulation is used to evaluate the limit state for chloride-induced depassivation in a two-step process: First, for each iteration and evaluation time t, the maximum of the chloride concentration $C(x,t)_{max}$ at the specified depth from the exposed surface x is identified for the whole domain using the reactive transport model described in Section 2.2. Note, that due to local variability of stress and damage, and due to the meso-scale modeling approach, the chloride concentration varies locally. Subsequently, the probability of exceeding the critical chloride concentration is determined using Eq. 18 by comparing the conservatively chosen chloride concentration $C(x,t)_{max}$ to the critical chloride content C_{crit}. This limit state is selected because local chloride-induced depassivation can trigger critical pitting corrosion.

In this study, Monte Carlo Simulation with 1000 samples per case is employed to evaluate the limit state.

3 CASE STUDY

In this study, the influence of mechanical loading on chloride diffusion in concrete beams is investigated using a four-point bending test. For this two mix designs are compared. Furthermore, this case study explores how internal stress levels influence chloride ingress and subsequently the depassivation of reinforcement.

3.1 Study setup

Subject of the case study are lab-scale, unreinforced concrete beams with the dimensions of 10 cm x 10 cm x 35 cm (h x b x l), based on the specifications outlined in DIN EN 12390-5 [26]. The mix design of both concretes (C50 and C35) is given in Table 3. The aggregate diameters and volumetric fractions are based on the sieve curve given in Table 4.

Table 3: Concrete mix design of C50 and C35

Type	Mass Fraction	Vol. Fraction
OPC	320 kg/m³	10.3 Vol.-%
Water	160 kg/m³	16.00 Vol.-%
Aggregates	1851 kg/m³	71.7 Vol.-%
Air content	-	2 Vol.-%

Table 4: Sieve Curve AB16 used for the geometry of mesoscale model of C50 and C35

Particle Diameter	Fraction Passing
16 mm	100 %
8 mm	68 %
4 mm	46 %

First, an unloaded concrete beam is compared to two distinct loading scenarios. These scenarios represent 40 % and 60 % of the beam's maximum load capacity, remaining below the threshold for micro-cracking. Second, a high-quality concrete with the mechanical properties of grade C50 is compared with a poor-quality concrete. The low-quality concrete possesses roughly 70 % of the strength of the high-quality concrete, which equals the mechanical properties of a grade C35.

All beams are then subjected to a 3 % NaCl solution at the tension side of the beam. All other sides are assumed to be sealed, allowing the chloride diffusion only from one surface of the beam. The specified depth from the exposed surface x, where the amount of chloride is evaluated, is assumed to be 0.035 m. This is chosen to be the critical chloride ingress depth, which usually equals the cover depth over the reinforcement.

3.2 Material properties

In the mechnaical simulation steel roller pins are used as bearings of the four-point bending test. The steel is characterized by a Young's modulus of 200 GPa and a Poisson's ratio of 0.33.

The mechanical properties of the coarse aggregates are kept constant for all simulations, with a Young's modulus of 70 GPa and a Poisson's ratio of 0.2. The mechanical properties of C50 and C35 concretes are provided in Table 5 and Table 6, respectively. Some mechanical properties of the mortar are adjusted to ensure that the stress-strain curve of the mesoscale model meets the requirements (E_{ci}, f_{ctm}) of the *fib* Model Code 2010 [27]. The stress-strain curve for uniaxial tension of C50 and C35 are shown in Figure 3. No failure of the mortar in compression is anticipated; therefore, the Mazars damage parameters for compression are kept constant at $A_c = 1.2$ and $B_c = 1000$. The regularization parameter l_0 is also maintained at 5.8 mm, and the shear exponent β is fixed at 1.0.

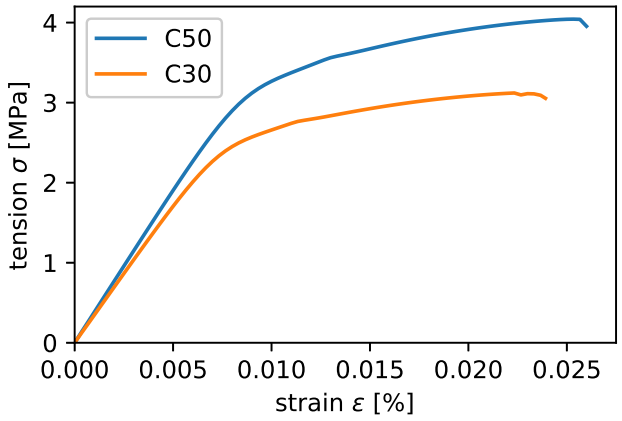

Figure 3: Stress-strain-diagram of the simulated concretes in uniaxial tension

Table 5: Mechanical properties C50

Property	Value	Source
modulus of elasticity of Concrete E_{ci}	38.6 GPa	[27]
tensile strength of Concrete f_{ctm}	4.1 MPa	[27]
modulus of elasticity of Mortar	26.8 GPa	fitted
Mazars damage parameter A_t	1.1	fitted
Mazars damage parameter B_t	3400	fitted
Mazars damage parameter κ_0	$1.3 \cdot 10^{-4}$	fitted

Table 6: Mechanical properties C35

Property	Value	Source
modulus of elasticity of Concrete E_{ci}	35.0 GPa	[27]
tensile strength of Concrete f_{ctm}	3.2 MPa	[27]
modulus of elasticity of Mortar	23.4 GPa	fitted
Mazars damage parameter A_t	1.0	fitted
Mazars damage parameter B_t	3800	fitted
Mazars damage parameter κ_0	$1.15 \cdot 10^{-4}$	fitted

For the probabilistic chloride diffusion simulation ordinary Portland cement concrete was assumed. The cement paste is assumed to contain 31.5 w.% C-S-H and 8.14 w.% AFm phase by mass paste. In the probabilistic analysis, these fractions are modeled as normally distributed with a standard deviation of 10 % of their mean values. Additionally, the w/b-ratio is considered normally distributed with a standard deviation of 5 % of its mean to account for uncertainties in the mix design. For service life prediction the critical chloride content C_{crit} is assumed to be beta distributed with a mean value of 0.6 w.% binder and a standard deviation of 0.15 w.% binder [1].

3.3 Boundary and transition conditions

For the four-point bending test, the boundary conditions are defined by the steel pins. The bottom roller pins are modeled with a frictional contact interface, assuming a static friction coefficient between concrete and steel μ of 0.2. The lowest point of the bottom rollers is constrained to zero displacement. Adhesive contact is assumed for the top rollers, where an increasing displacement is applied at the top of the rollers.

The chloride diffusion in the unloaded and loaded beams subjected to a 3.0 w.% NaCl solution is investigated. A Dirichlet boundary condition with the exposure solution is applied to the tension side of the beam and all other boundaries have no flux boundary conditions. This resembles realistic boundaries conditions in lab experiments.

3.4 Definition of loading conditions

To define the loading scenarios of 40 % and 60 %, the maximum force that can be applied was determined for the C50 concrete in a displacement-driven four-point bending simulation. The force-displacement curves of these preliminary simulations are presented in Figure 4.

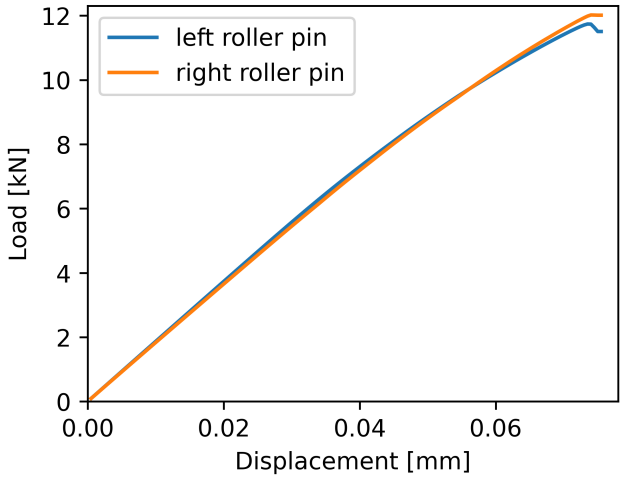

Figure 4: Load displacement curve of the concrete beam

The maximum load at the pins before softening is 11.7 kN on the left and 12.0 kN on the right. Therefore, the applied forces on the pins for the stress levels of 40 % and 60 % are set to 4.8 kN and 7.1 kN, respectively. To compare the high-quality concrete (C50) with the low-quality concrete (C35) the same load of 7.1 kN is applied to the pins corresponding to 60 % stress level.

4 RESULTS

The load states of 40 % and 60 % do not cause any damage in the mortar of the high-quality concrete (C50). However, with the low-quality material properties (C35), a load of 7.1 kN applied to the pins induces damage in the tension zone of the beam (Figure 5).

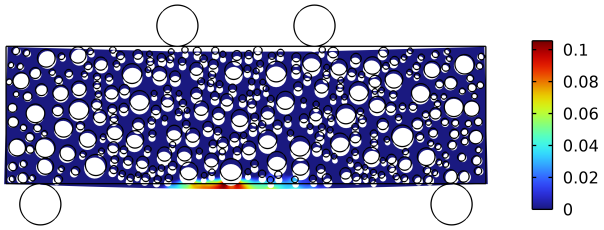

Figure 5: Distribution of scalar damage d for for simulation with lower strength and a loading of 7.1 kN

Consequently, the damage d and the increased local stress level λ lead to a rise in the diffusion coefficients $D_{e,load}$ within the tension zone, as shown in Figure 6.

Higher load levels not only increase the diffusion coefficient, but also expand the area where the diffusion coefficient is significantly higher. Reduced diffusion coefficients are found only near the pins in all loading scenarios due to localized compression from the applied load. Due to the low stress levels in the compression zone of the beam, the diffusion coefficient is negligibly affected.

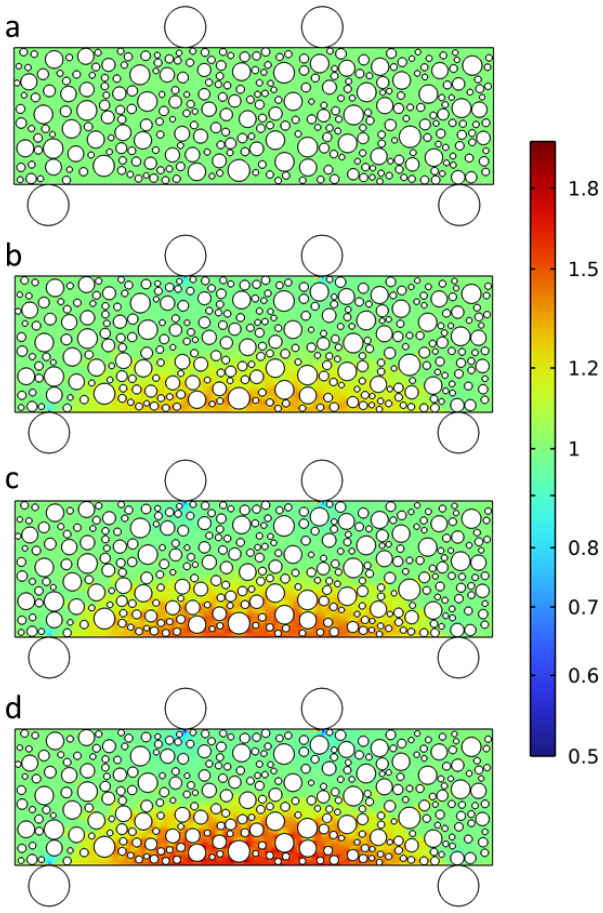

Figure 6: Mean values of $D_{e,load}$ normalized with D_e for **a**: unloaded condition, **b**: 4.8 kN on high-quality concrete , **c**: 7.1 kN on high-quality concrete, and **d**: 7.1 kN on low-quality concrete

In the tension zone at a load of 4.8 kN (Figure 6b), the effective diffusion coefficient shows a localized increase. Maximum values are observed between closely horizontally adjacent aggregates. This occurs because the ITZ remains intact at this load level, and the stiffer aggregates attract a greater proportion of the applied stress. At a load of 7.1 kN (Figure 6c-d), the ITZ in high-stress areas is damaged, leading to a more homogeneous increase in the effective diffusion coefficient throughout the mortar. In the case of 7.1 kN loading applied to the low-quality concrete (Figure 6d), damage appears in the mortar near the bottom of the beam, causing a further increase in the diffusion coefficient close to the exposed surface.

The distribution of total chloride content

C_{total} after three years at a load of 7.1 kN is shown in Figure 7. Here, the normal distributed random variables are set to their mean values.

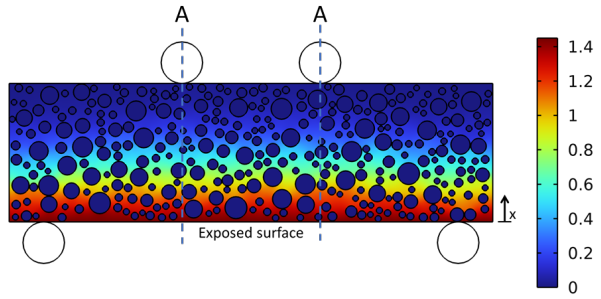

Figure 7: Mass fraction of total chloride C_{total} related to cement content [w.-% cement] after 3 years loaded with 7.1 kN

To compare the total chloride content C_{total} of the different loading scenarios more detailed, 1D chloride profiles are presented in Figure 8.

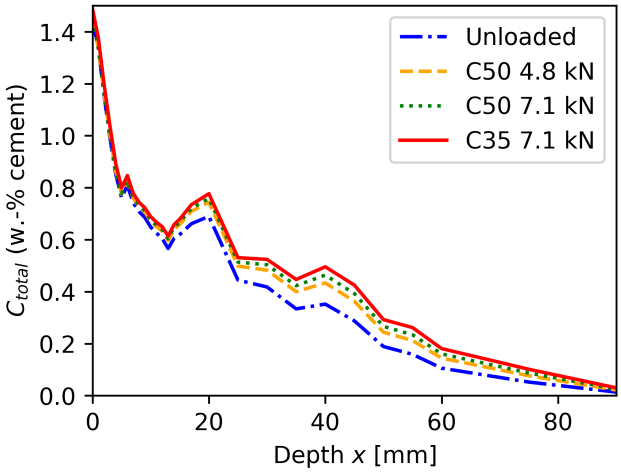

Figure 8: Average profiles of total chloride content C_{total} in between top pins after 3 years

For this, the average C_{total} is calculated at the center of the beam at section A-A at various depths, so that only the visible peaks in the 1D profiles are due to the inhomogeneous structure of the concrete, which consists of mortar and randomly distributed aggregates. Contrary to previously discussed experimental observations, the concentration near the surface remains the same independent of the loading scenario. However, at greater depths, the chloride content is significantly higher in the loaded scenarios. It is noteworthy that regardless of the diffusion time, the differences in chloride content between the loaded and unloaded scenarios are more pronounced than the differences observed between the different loaded scenarios.

The probability for exceeding the critical chloride content p_{dep} at 0.035 m depth is calculated using Eq. 18 for up to ten years and presented in Figure 9.

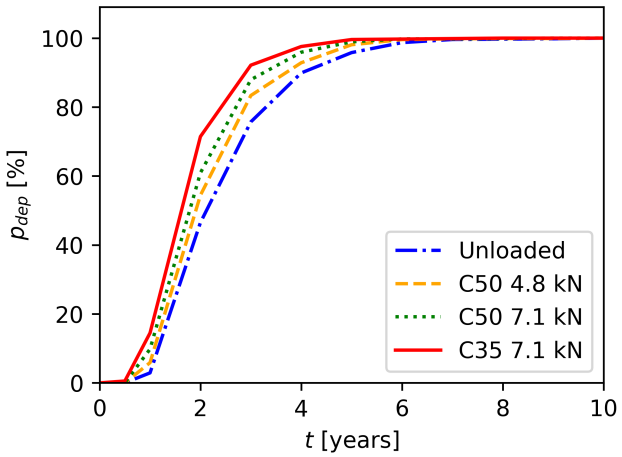

Figure 9: Probability for exceeding the critical chloride content p_{dep} at 0.035 m depth with time

In general, probability for exceeding the critical chloride content (and therefore the probability of depassivation of reinforcement) is the lowest for the unloaded concrete and increases with increased mechanical loading, regardless of the evaluation time. The highest probability is observed for the low-quality concrete in the high loading scenario (C35 7.1 kN). A probability of 99 % is reached after five to seven years, with "C35 7.1 kN" converging the fastest and the unloaded scenario takes the longest time.

In practice, it is essential to quantify the reduction in time to depassivation for a given level of reliability. To this end, the time required for the depassivation probability to exceed 30 % (reliability index $\beta \approx 0.5$), as proposed by [28], is evaluated for all cases. For the unloaded case, which serves as a reference, this time is 1.62 years. For high quality concrete subjected

to a load of 4.8 kN, the duration is reduced to 1.49 years, which is a reduction of 8 %. At a higher load of 7.1 kN, the duration is further reduced to 1.39 years (14 % less). For low quality concrete, the time to depassivation is further reduced to 1.27 years (22 % less).

5 CONCLUSION

The model predicts altered chloride diffusivity in loaded concrete by accounting for a stress-dependent diffusion coefficient, and for a change in mortar porosity due to stress-induced damage particularly in areas of higher stress. This effect is more pronounced in low-quality concrete, where high loads caused damage to the mortar and ITZ, leading to a more homogeneous rise in diffusivity. As a result, chloride ingress progresses further and faster in loaded scenarios, leading to a reduction in predicted life of up to 22 %.

In this study, the model uses a correlation of normalised diffusion coefficients with stress levels based on experimental studies of [5,9,10, 22,23]. As a first approximation to account for the influence of stress levels on chloride ingress on a mesoscopic scale, linear relationships are assumed in Eq. 14 and Eq. 15. This may be an oversimplification. Therefore, other physically consistent functions should be investigated.

Furthermore, the diffusion in the ITZ was neglected in this study. This is because it was found that for unloaded and uncracked OPC concretes, chloride diffusion within the ITZ is negligible [18]. However, it needs to be investigated whether diffusion in the damaged ITZ should be considered in further studies.

In this case study, the beam size was chosen to resemble a realistic lab setup, in order to enable bending tests for validating the simulations. However, in this setup the influence of compression in negligible. To investigate the latter, compression dominated load scenarios should be included in further studies and validated with experimental studies comparable to the setup shown in [28].

This study presents a mesoscale model integrating fracture mechanics, reactive chloride transport, and probabilistic analysis to evaluate the influence of mechanical loading on chloride ingress in concrete structures. The model captures the interplay between stress-induced changes on the diffusion coefficient, and damaged-altered porosity providing a detailed understanding of how tensile and compressive loading impact chloride transport and depassivation probability. The probabilistic Monte Carlo analysis demonstrated how the variability in material properties can be accounted for in service life predictions. The case study demonstrates that mechanical loading accelerates chloride-induced depassivation.

In conclusion, the framework provides initial insights into a performance-based probabilistic durability assessment by accounting for load-induced stress in concrete structures exposed to chloride environments.

REFERENCES

[1] International Federation for Structural Concrete. *Model Code for Service Life Design: Bulletin no 34*. Bulletin // International Federation for Structural Concrete Model code. International Federation for Structural Concrete (fib), Lausanne, 2006.

[2] Hugo Egüez Álava, Eleni Tsangouri, Nele de Belie, and Geert de Schutter. Chloride interaction with concretes subjected to a permanent splitting tensile stress level of 65%. *Construction and Building Materials*, 127:527–538, 2016.

[3] Fu Xiang Jiang, Lei Xin, Tie Jun Zhao, and Xiao Mei Wan. Inner damage and anti-chloride penetration of high-performance concrete under axial tensile load. *Advanced Materials Research*, 261-263:1210–1214, 2011.

[4] Dong Hun Kim, Kazunori Shimura, and Takashi Horiguchi. Effect of tensile loading on chloride penetration of concrete mixed with granulated blast furnace slag.

Journal of Advanced Concrete Technology, 8(1):27–34, 2010.

[5] Yun-sheng Zhang, Wei Sun, Zhi-yong Liu, and Shu-dong Chen. One and two dimensional chloride ion diffusion of fly ash concrete under flexural stress. *Journal of Zhejiang University-SCIENCE A*, 12(9):692–701, 2011.

[6] Walid A. Al-Kutti. *Simulation of Chloride Transport in Concrete with Stress Induced Damage*. Dissertation, King Fahd University of Petroleum and Minerals, Dhahran, 2011.

[7] Li Guoping, Hu Fangjian, and Wu Yongxian. Chloride ion penetration in stressed concrete. *Journal of Materials in Civil Engineering*, 23(8):1145–1153, 2011.

[8] Yan Yao, Ling Wang, Folker H. Wittmann, Nele de Belie, Erik Schlangen, Hugo Eguez Alava, Zhendi Wang, Sylvia Kessler, Christoph Gehlen, Balqis Md. Yunus, Juan Li, Weihong Li, Max. J. Setzer, Feng Xing, and Yin Cao. Test methods to determine durability of concrete under combined environmental actions and mechanical load: final report of rilem tc 246-tdc. *Materials and Structures*, 50(2), 2017.

[9] Xiaokang Cheng, Jianxin Peng, C. S. Cai, and Jianren Zhang. Experimental study on chloride ion diffusion in concrete under uniaxial and biaxial sustained stress. *Materials (Basel, Switzerland)*, 13(24), 2020.

[10] Hailong Wang, Chunhua Lu, Weiliang Jin, and Yun Bai. Effect of external loads on chloride transport in concrete. *Journal of Materials in Civil Engineering*, 23(7):1043–1049, 2011.

[11] Jun Xu, Fumin Li, Jie Zhao, and Lang Huang. Model of time-dependent and stress-dependent chloride penetration of concrete under sustained axial pressure in the marine environment. *Construction and Building Materials*, 170:207–216, 2018.

[12] Yan Yao, Ling Wang, Folker H. Wittmann, Nele de Belie, Erik Schlangen, Christoph Gehlen, Zhendi Wang, Hugo Eguez Alava, Yin Cao, Balqis MD Yunus, and Juan Li. Recommendation of rilem tc 246-tdc: test methods to determine durability of concrete under combined environmental actions and mechanical load: Test method to determine the effect of applied stress on chloride diffusion. *Materials and Structures*, 50(2), 2017.

[13] Comsol multiphysics® v. 6.2. www.comsol.com.

[14] Jacky Mazars. A description of micro- and macroscale damage of concrete structures. *Engineering Fracture Mechanics*, 25(5-6):729–737, 1986.

[15] Leong Hien Poh and Gang Sun. Localizing gradient damage model with decreasing interactions. *International Journal for Numerical Methods in Engineering*, 110(6):503–522, May 2017.

[16] S. C. Seetharam, E. Laloy, A. Jivkov, L. Yu, Q. T. Phung, N. P. Pham, B. Kursten, and F. Druyts. A mesoscale framework for analysis of corrosion induced damage of concrete. *Construction and Building Materials*, 216:347–361, 2019.

[17] Annika L. Schultheiß, Ravi A. Patel, and Frank Dehn. A probabilistic approach to service life prediction: Comparing a reactive transport model with the fib chloride model. In *PROCEEDINGS OF THE RILEM SPRING CONVENTION AND CONFERENCE 2024*, pages 339–347, [S.l.], 2024. SPRINGER INTERNATIONAL PU.

[18] Ravi A. Patel, Quoc Tri Phung, Suresh C. Seetharam, Janez Perko, Diederik

Jacques, Norbert Maes, Geert de Schutter, Guang Ye, and Klaas van Breugel. Diffusivity of saturated ordinary portland cement-based materials: A critical review of experimental and analytical modelling approaches. *Cement and Concrete Research*, 90:52–72, 2016.

[19] S. C. Seetharam, R. A. Patel, J. Perko, and D. Jacques. Quantification of leaching kinetics in opc mortars via a mesoscale model. *Construction and Building Materials*, 180:614–628, 2018.

[20] Torben C. Hansen. Physical structure of hardened cement paste. a classical approach. *Matériaux et Constructions*, 19(6):423–436, 1986.

[21] S. Bejaoui and B. Bary. Modeling of the link between microstructure and effective diffusivity of cement pastes using a simplified composite model. *Cement and Concrete Research*, 37(3):469–480, 2007.

[22] Jian Wang, Pui-Lam Ng, Weishan WANG, Jinsheng Du, and Jianyong SONG. Modelling chloride diffusion in concrete with influence of concrete stress state. *Journal of Civil Engineering and Management*, 23(7):955–965, 2017.

[23] L. C. Wang and J. Z. Wang. Mesoscale simulation of chloride diffusion in concrete subjected to flexural loading. *Advances in Structural Engineering*, 17(4):561–571, 2014.

[24] *Zement-Taschenbuch*, volume 51 of *Zement-Taschenbuch*. Verlag Bau + Technik, Düsseldorf, 51. aufl. edition, 2008.

[25] E N Landis and J E Bolander. Explicit representation of physical processes in concrete fracture. *Journal of Physics D: Applied Physics*, 42(21):214002, November 2009.

[26] DIN EN 12390-5:2019-10, Prüfung von Festbeton_- Teil_5: Biegezugfestigkeit von Probekörpern; Deutsche Fassung EN_12390-5:2019.

[27] Comité euro-international du béton, editor. *Fib model code for concrete structures 2010*. Ernst & Sohn, Berlin, 2013.

[28] Yan Yao, Ling Wang, Folker H. Wittmann, Nele de Belie, Erik Schlangen, Hugo Eguez Alava, Zhendi Wang, Sylvia Kessler, Christoph Gehlen, Balqis Md. Yunus, Juan Li, Weihong Li, Max. J. Setzer, Feng Xing, and Yin Cao. Final report of rilem tc 246-tdc.